Ab initio calculations of inelastic transport in atomic/molecular junctions and waveguide effects

2008 J. Phys.: Condens. Matter 20 224023

(http://iopscience.iop.org/0953-8984/20/22/224023)

IOP PUBLISHING JOURNAL OF PHYSICS: CONDENSED MATTER

J. Phys.: Condens. Matter **20** (2008) 224023 (7pp) doi:10.1088/0953-8984/20/22/224023

Ab initio calculations of inelastic transport in atomic/molecular junctions and waveguide effects

Hisao Nakamura

Department of Chemical System Engineering, Graduate School of Engineering,
The University of Tokyo, 113-8656, Japan

E-mail: nakamura@tcl.t.u-tokyo.ac.jp

Received 8 November 2007, in final form 27 December 2007
Published 13 May 2008
Online at stacks.iop.org/JPhysCM/20/224023

Abstract

To model electron transport through atomic/molecular junctions, we propose an efficient method using nonequilibrium Green's function theory combined with density functional theory. We have applied our method to atomic gold wire with gold electrodes and calculated elastic and inelastic conductance. We find that quantum confinement of the electrodes is an important issue for electron transport because of waveguide effects. The results show the important role of the phase factors between the modeled electrodes and the contact region.

1. Introduction

There has been progress in the application of conduction by atomic wires or molecular junctions to new devices [1–4] and single-molecule spectroscopic techniques, such as inelastic electron tunneling spectroscopy (IETS) [5–13] Generally, it is difficult to manipulate or specify the atomic structure for the junction (contact region) experimentally, and therefore several groups have performed *ab initio* calculations of transport for realistic electrode–molecule–electrode systems using nonequilibrium Green's function theory (NEGF) combined with density functional theory (DFT) [14–18] Theoretical treatment of the electrodes often depends on an adopted model of the contact region and an *ab initio* method, such as cluster approximation or the periodic slab model. The latter is more suitable for modeling systems which contain sufficiently large (infinite to the direction parallel to the surface) electrodes. However, the computational cost of the self-consistent-field (SCF) in NEGF (NEGF-SCF) is usually large, and it is sometimes difficult to get convergence of the SCF.

Recently we proposed a new efficient algorithm for NEGF-SCF based on the molecular orbital (MO) expansion and named 'efficient MO approach' [16] Our scheme consists of three main features: (i) perturbation expansion of the Green's function in the MO basis, (ii) a truncated MO space scheme to estimate the density matrix, and (iii) introduction of the embedding potential to reproduce the contribution caused by the long-range bulk potential. In the present paper we develop the method by improving two points. The first is by introducing the correction term of the density matrix combined with a slight modification of the embedding potential in order to make the procedures of NEGF-SCF and the constructed embedding potential consistent. As the second improvement, we propose an accurate $O(N)$ method to estimate self-energy matrices for semi-infinite electrodes. These two improvements allow numerically stable NEGF-SCF calculations and therefore lead to acceleration of the convergence as well as high computational efficiency.

As test calculations, we apply our method to inelastic transport in gold atomic wire with gold electrodes. To estimate the contribution of electron–phonon interactions to the conductance, we incorporate our new method in the lowest order expansion (LOE) framework, proposed by several groups [19–21]. In the atomic/molecular junctions, quantum confinement plays important role in the transport. Ke *et al* showed that the behavior of transport through the whole system depends not only on contact but also on the electrode itself as a result of quantum confinement [22]. By performing the above test calculations, we report that the quantum confinement and waveguide effects contribute to the change of conductance caused by electron–phonon scattering as well as ballistic transmission coefficients.

The organization of the paper is as follows. In section 2, we provide the theoretical framework and computational scheme. The theoretical background of the NEGF and LOE formalism is reviewed in section 2.1, and a brief review

of our efficient MO approach is given in section 2.2. In section 2.3, the two improvements, the correction factor of the density matrix and the $O(N)$ algorithm for calculating a self-energy matrix, are shown. The test calculations and analysis of waveguide effects are described in section 3, and our conclusion is summarized in section 4.

2. Theory

2.1. NEGF and LOE formalism for inelastic transport

First we briefly describe the LOE formalism based on the NEGF framework. The details are given in [21, 23]. First we introduce the Hamiltonian of electrons coupled to vibrational modes as follows:

$$\begin{aligned} H &= H^{\mathrm{e}} + H^{\mathrm{ph}} + H^{\mathrm{eph}} \\ H^{\mathrm{e}} &= \sum_{m,m'} H_{\mu\mu'} d_{\mu}^{\dagger} d_{\mu'} \\ H^{\mathrm{ph}} &= \sum_{\alpha} \Omega_{\alpha} b_{\alpha}^{\dagger} b_{\alpha} \\ H^{\mathrm{eph}} &= \sum_{\alpha,m,m'} M_{\mu\mu'}^{\alpha} d_{\mu}^{\dagger} d_{\mu'} (b_{\alpha}^{\dagger} + b_{\alpha}), \end{aligned} \tag{1}$$

where $d_{\mu}^{\dagger}$ is a creation operator for an electron, and $H_{\mu\mu'}$ is the matrix element of the mean-field Hamiltonian in the atomic orbital (AO) basis. The operator $b_{\alpha}^{\dagger}$ is the phonon creation operator relating to the vibrational mode α, which has the normal mode coordinate Q_{α} and frequency Ω_{α}. The matrix element $M_{\mu\mu'}^{\alpha}$ is the electron–phonon (e–ph) coupling. We adopt the atomic unit, i.e. $e = \hbar = 1$.

To perform practical *ab initio* calculations, the system in question should be projected to the finite region, denoted as C, and further divided into three parts L, c, and R, which relate to the left lead part, the central region, and the right lead part, respectively. Since the Hamiltonian includes (semi-infinite) electrodes, these semi-infinite electrode parts connected to L/R regions are renormalized to the L and R region as the lead self-energy terms such as Σ_L and Σ_R: thus the Green's functions are expanded only in the C region. The e–ph interactions are incorporated into the Green's functions by using e–ph (lesser and retarded) self-energy terms. In the present formalism, the e–ph interactions are assumed to be restricted in the C region: thus the coupling $M_{\mu\mu'}^{\alpha}$ is defined only in the C region. Furthermore the normal mode is obtained by means of a frozen-phonon [24], where displaced atoms are atoms in the c region (or its subpart) relating to the bridge molecule (or wire) denoted as a 'vibrational box' [25]. When the e–ph coupling is weak, the e–ph self-energies for an electron interacting with the α mode can be expanded in term of the Hartree–Fock diagrams as follows: [23, 26, 27]

$$\begin{aligned} \mathbf{\Sigma}_{\alpha:\mathrm{eph}}^{<}(E) &= \frac{\mathrm{i}}{2\pi} \int \mathrm{d}\omega D_{\alpha}^{<}(\omega) \mathbf{M}^{\alpha} \mathbf{G}^{<}(E-\omega) \mathbf{M}^{\alpha} \\ \mathbf{\Sigma}_{\alpha:\mathrm{eph}}(E) &= \frac{\mathrm{i}}{2\pi} \int \mathrm{d}\omega \Big\{ D_{\alpha}^{<}(\omega) \left[\mathbf{M}^{\alpha} \mathbf{G}(E-\omega) \mathbf{M}^{\alpha} \right] \\ &\quad + D_{\alpha}(\omega) \left[\mathbf{M}^{\alpha} \mathbf{G}^{>}(E-\omega) \mathbf{M}^{\alpha} \right] \\ &\quad - D_{\alpha}(0) \mathbf{M}^{\alpha} \mathrm{Tr} \left[\mathbf{M}^{\alpha} \mathbf{G}^{<}(\omega) \mathbf{M}^{\alpha} \right] \Big\} \end{aligned} \tag{2}$$

where the symbols '$<$' and '$>$' represent the lesser and greater functions as is Green's functions for electrons $G(E)$ and for phonons D_{α}, and we adopt the matrix representation for convenience. When focused phonon modes are plural but couplings between them can be omitted, the e–ph self-energies are simply the sum of self-energies for each mode. We denote the total e–ph self-energies as $\Sigma_{\mathrm{eph}}^{<}$ and Σ_{eph}.

The Green's functions are obtained by the Dyson equation (for the retarded Green's function) and the Keldysh–Kadanoff–Baym (KKB) equation (for the lesser Green's function), formally

$$\begin{aligned} \mathbf{G}^{<}(E) &= \mathbf{G}(E)(\mathbf{\Sigma}_L^{<} + \mathbf{\Sigma}_R^{<} + \mathbf{\Sigma}_{\mathrm{eph}}^{<}) \mathbf{G}^{\dagger} \\ \mathbf{G}(E) &= \tilde{\mathbf{G}}(E) + \tilde{\mathbf{G}}(E) \mathbf{\Sigma}_{\mathrm{eph}}(E) \mathbf{G}(E) \end{aligned} \tag{3}$$

where $\tilde{G}(E)$ is the solution of the Dyson equation without e–ph interactions, i.e. $\tilde{G}(E) = (E - H - \Sigma_L - \Sigma_R)^{-1}$. The total current (including the spin factor) for the applied bias V_{b} can be expressed as follows:

$$I(V_{\mathrm{b}}) = \frac{1}{\pi} \int \mathrm{d}E \mathrm{Tr} \left[\mathbf{\Sigma}_L^{<}(E) \mathbf{G}^{>}(E) - \mathbf{\Sigma}_L^{>} \mathbf{G}^{<}(E) \right]. \tag{4}$$

Since e–ph interactions contribute to the nonequilibrium states of phonons, similar equations can be applied to the phonon Green's functions. There are several forms for evaluating e–ph self-energies within Hartree–Fock diagrams. In the present study, we adopt the LOE approximation [19–21]. The LOE is basically the second-order perturbation expansion with respect to the e–ph couplings. However, it contains the term of nonequilibrium phonon distribution function, which is defined by the lesser phonon Green's function. Therefore the final form includes some terms of higher than second order partially to represent nonequilibrium vibrational heating. As a result the LOE can give qualitatively correct properties of the IETS signal although it is convenient to analyze numerical results in the sense of the perturbation theory [26].

In the LOE, the total current can be represented as the sum of three terms as follows:

$$I = I_0^{\mathrm{el}} + \delta I^{\mathrm{el}} + I^{\mathrm{inel}}. \tag{5}$$

The elastic part consists of the ballistic term I_0^{el} and the remaining term δI^{el}, which relates to the complicated electron–phonon scatterings such as the background scatterings. The term I^{inel} is inelastic current due to inelastic scatterings. The terms I_0^{el}, δI^{el}, and I^{inel} are expressed in terms of $\tilde{G}(E)$, i.e. the result of NEGF without e–ph interactions. The rigorous expressions for the LOE are derived by Viljas *et al*, and each currents I_0^{el}, δI^{el}, I^{inel} can be given by equations (E1), (E2), and (E3), respectively, in [21]. In the present calculations, we adopt their expression although we omitted the third term in the above (E3). The currents δI^{el} and I^{inel} contain the voltage-dependent nonequilibrium phonon distribution function, $N_{\alpha}(\omega, V_{\mathrm{b}}, T{:}\eta)$, where ω, T, and η are (phonon) energy, bath temperature, and the broadening parameter for the phonon Green's function. We adopt the conventional expression for N_{α}, which is also given in equations (14)–(16) in [21], to calculate the above currents.

2.2. Efficient MO approach based on truncated MO space

To perform practical *ab initio* calculation, we employ the DFT framework to construct the Hamiltonian by means of the Kohn–Sham (KS) Hamiltonian. For later use, we give the explicit matrix representation for the Green's function $\tilde{G}(E)$ as follows:

$$\tilde{\mathbf{G}}_{\mathrm{CC}} = \begin{pmatrix} E\mathbf{S}_{\mathrm{LL}} - \mathbf{H}_{\mathrm{LL}} - \mathbf{\Sigma}_L(E) & E\mathbf{S}_{Lc} - \mathbf{H}_{Lc} & 0 \\ E\mathbf{S}_{Lc}^{\dagger} - \mathbf{H}_{Lc}^{\dagger} & E\mathbf{S}_{\mathrm{cc}} - \mathbf{H}_{\mathrm{cc}} & E\mathbf{S}_{\mathrm{cR}} - \mathbf{H}_{\mathrm{cR}} \\ 0 & E\mathbf{S}_{\mathrm{cR}}^{\dagger} - \mathbf{H}_{\mathrm{cR}}^{\dagger} & E\mathbf{S}_{\mathrm{RR}} - \mathbf{H}_{\mathrm{RR}} - \mathbf{\Sigma}_R(E) \end{pmatrix}^{-1} \tag{6}$$

in which the direct couplings between the L and R regions are 0. This will be valid as long as the c region is sufficiently large because we employ the localized AO basis set. The matrix $\boldsymbol{S}$ is the overlap matrix between AOs. In our efficient MO approach, the NEGF-SCF calculation is performed by the MO basis set, which are eigenstates of the matrix $\mathbf{H}_{\mathrm{CC}}$ and labeled by indices I, J etc. In the MO basis, the perturbation expansion of the Green's function (PT-GF), which is denoted as $\tilde{G}^{\mathrm{PT}}(E)$ and expressed as the diagonal matrix, is a good first approximation. Following [16], the matrix form of $\tilde{G}^{\mathrm{PT}}$ is represented as follows:

$$\tilde{\mathbf{G}}^{\mathrm{PT}}_{\mathrm{CC}}(E) = \mathrm{diag}\left[\left\{E - \varepsilon_I^0 - \frac{\mathrm{i}}{2}\left(\mathbf{\Gamma}_{\mathrm{L,II}}(\varepsilon_I^0) + \mathbf{\Gamma}_{\mathrm{R,II}}(\varepsilon_I^0)\right)\right\}^{-1}\right] \tag{7}$$

where ε_I^0 is the MO energy and $\Gamma_{\mathrm{L/R}} = -2\,\mathrm{Im}\,\mathbf{\Sigma}_{\mathrm{L/R}}$. If one prefers the wide-band-limit approximation, one can replace $\Gamma_{\mathrm{L/R,II}}(\varepsilon_I^0)$ to $\Gamma_{\mathrm{L/R,II}}(\varepsilon_{\mathrm{F}})$, where ε_{F} is the Fermi energy. From the KKB equation, the PT-GF for the lesser function can also be obtained as the diagonal matrix, $\tilde{\mathbf{G}}^{\mathrm{PT}<}_{\mathrm{CC}}$.

Since the density matrix is obtained by the energy integral of the lesser Green's function, the density matrix in the MO basis is also diagonal, this is an electron occupation number for MO I, which is denoted as d_I: i.e.

$$\mathrm{diag}\,[d_I] = \frac{-\mathrm{i}}{2\pi}\int \mathrm{d}E\tilde{\mathbf{G}}^{\mathrm{PT}<}_{\mathrm{CC}}(E). \tag{8}$$

Numerical evaluation of d_I is much easier than calculating the density matrix in the AO basis, and it reduces the computational cost drastically. After each NEGF-SCF cycle, one can transform the density matrix from the MO to the AO basis representation to update the Hamiltonian.

To make the NEGF-SCF step even more efficient we proposed the 'truncated MO space' idea, and applied it to the present calculations. The details of the procedure and justification can also be found in [16], as well as the details of the scheme. Here we only briefly follow the outline of the concept. If the MO energy is much lower than the Fermi level, the electron occupation number will always be 1 (or 2 by including the spin factor). On the other hand, the occupation will be always zero if the MO energy is much higher than the Fermi level. Therefore only d_I in the 'active space' should be determined by the NEGF-SCF. Therefore the active space is a small part of the whole MO space. This is the central issue of the truncated MO space concept. The active space can be defined by the MO energies in the zero-bias limit and should be large enough to cover the energy region relating to the focused maximum/minimum bias. Usually the applied bias is within a few volts; thus the active space is smaller than about 10% of the whole MO space. By combining the truncated MO scheme with the PT-GF approximation in the above equations (7) and (8), one can further reduce the computational cost of the numerical integral calculations because the estimation of equation (8) requires only the active MOs, otherwise it is zero or one. Here we note that the use of PT-GFs is only for the NEGF-SCF step, and calculations of properties should be carried out using the full Green's function matrix after the SCF is converged [16].

2.3. Correction of density matrix and $O(N)$ method to calculate a self-energy matrix

In this subsection we give two improvements of our algorithm, the correction factor for the density matrix and the $O(N)$ method for calculations of a lead self-energy matrix. The first includes a minor modification relating to the embedding potential method, which was one of schemes in our previous efficient MO approach. In order to introduce the embedding potential we need to define the W region, which should be sufficiently large for the C region to reproduce the contribution of the long-range potential on the C region, which is created by the standard KS-DFT calculation for the W region with the slab model. The need for an embedding potential and its justification are also given in [16] together with the detailed procedures. Therefore we describe the minimum needed to explain the correction factor.

To define the correction factor, we rewrite a matrix representation of the embedding potential in [16] as follows:

$$\mathbf{V}^{\mathrm{emb}}_{\mathrm{CC}} = \mathbf{H}_{\mathrm{CC}}[W] - (\mathbf{T}_{\mathrm{CC}} + \mathbf{V}^{H}_{\mathrm{CC}}\{\mathbf{D}_{\mathrm{CC}}[W]\} + \mathbf{V}^{\mathrm{XC}}_{\mathrm{CC}}\{\mathbf{D}_{\mathrm{CC}}[W]\}) \tag{9}$$

where $\mathbf{H}_{\mathrm{CC}}[W]$ is the '*clipped*' matrix form the KS-SCF Hamiltonian for the W region (or with replacement of $\mathbf{H}_{\mathrm{LL}}$ and $\mathbf{H}_{\mathrm{RR}}$ parts relating to bulk Hamiltonian matrices.). The notation $\mathbf{V}^{\mathrm{H/XC}}_{\mathrm{CC}}\{\mathbf{D}_{\mathrm{CC}}\}$ represents that the Hartree/XC potential matrices are calculated by using the density matrix $\mathbf{D}_{\mathrm{CC}}$. The matrix $\mathbf{D}_{\mathrm{CC}}[W]$ is the clipped matrix from the KS-SCF density matrix for the W region (or with replacement, as is the Hamiltonian). To make the resulting density matrices from the KS-SCF for the W region and from the NEGF-SCF by equation (8) (then transformed to AO basis) consistent with the zero-bias limit (i.e. $V_{\mathrm{b}} = 0$), we can introduce the correction factor $\Delta\mathbf{D}_{\mathrm{CC}}$ as follows:

$$\Delta\mathbf{D}_{\mathrm{CC}} = \mathbf{D}_{\mathrm{CC}}[W] + \frac{\mathrm{i}}{\pi}\int \mathrm{d}E\tilde{\mathbf{G}}^{<}_{\mathrm{CC}}(E)|_{V_{\mathrm{b}}=0} \tag{10}$$

where the second term on the right-hand side can be approximated by the use of PT-GFs for practical calculations, and we include a spin factor of 2. To update the Hamiltonian in the NEGF-SCF step for non-zero bias, the Hartree and XC potential terms are estimated by the corrected density matrix:

$$\mathbf{D}_{\mathrm{CC}} = \frac{-\mathrm{i}}{\pi}\int \mathrm{d}E\tilde{\mathbf{G}}^{<}_{\mathrm{CC}}(E) + \Delta\mathbf{D}_{\mathrm{CC}}. \tag{11}$$

The term $\Delta\mathbf{D}_{CC}$ enforces the consistency that $\mathbf{D}_{CC}[W]$ should agree with the resulting density matrix from NEGF-SCF in the zero-bias limit, which is the assumption made in order to introduce the embedding potential [16]. Usually $\Delta\mathbf{D}_{CC}$ should be close to the zero matrix. However, there are a few cases in which the integral $\int \mathrm{d}E\tilde{\mathbf{G}}^{<}_{CC}(E)$ is numerically unstable. For an instance, if the system is a completely one-dimensional chain system, van Hove singularity leads to an unphysical value for some energy grid points [28]. As another example, when metal–insulator gap-states (MIGS) or surface state orbitals exist close to the Fermi level, self-energy matrix elements are almost equal to 0, leading to numerical instability. The term $\Delta\mathbf{D}_{CC}$ eliminates such unphysical instability, which accidentally occurs in the SCF cycle, and gives faster convergence. Further details of the analysis and relations between the embedding potential and the correction factor of the density matrix will be given in elsewhere [29].

Next we incorporate the $O(N)$ scheme to evaluate self-energy matrices of electrodes combined with the tight-binding-layer (TBL) method by Sanvito *et al* [17, 30]. The basic strategy of the $O(N)$ scheme was proposed by Damle *et al* [31] and we extend it. We describe the method when the electrodes have a $N_{\mathrm{cell}} \times N_{\mathrm{cell}}$ structure with Γ point approximation as an example. Instead of calculating the self-energies of the $N_{\mathrm{cell}} \times N_{\mathrm{cell}}$ structure directly, one can use a Fourier expansion of the self-energies of the 1×1 structure, $\Sigma^0(\vec{k}_{\parallel})$, as follows:

$$\Sigma_{\mu'\nu'} = \sum_{\vec{k}_{\parallel}} \Sigma^0_{\mu\nu}(\vec{k}_{\parallel}) \mathrm{e}^{-\mathrm{i}\vec{k}_{\parallel}(\vec{R}'_{\mu}-\vec{R}'_{\nu})} \tag{12}$$

where μ' is the set of AOs of atoms in the $N_{\mathrm{cell}} \times N_{\mathrm{cell}}$ cell, but μ is in the unit 1×1 cell. The $\vec{k}_{\parallel}$ vector is a wavevector parallel to the surface, and sufficient numbers of $\vec{k}_{\parallel}$ should be sampled if the cell for Σ consists of a number of cells for Σ^0. Because equation (12) allows one to calculate two-dimensionally wide electrodes using only the self-energy matrices of the smaller unit cell, it provides the $O(N)$ algorithm.

However, simple use of equation (12) gives unphysical oscillation of physical properties such as transmission coefficients due to unphysical waveguide effects, and a careful treatment of the phase factors for one-electron wavefunctions is required to avoid unreasonable interference by summing all $\vec{k}_{\parallel}$. To determine a suitable relation between phase factors and interference explicitly, we introduce the 'phase matching condition' to connect the contact and electrodes as follows:

$$\vec{k}_{\parallel} \cdot (N_{\mathrm{cell}}\vec{t}) = 2n\pi \tag{13}$$

where $\vec{t}$ is a translational vector of the unit cell of the electrodes, and n is an integer. Recall that the two-dimensional periodic boundary condition for the $N_{\mathrm{cell}} \times N_{\mathrm{cell}}$ cell is incorporated within the Γ point approximation in the present scheme.

Finally we briefly comment on the problem of the Γ point approximation caused by the van Hove singularity, which was recently pointed out by Thygesen and Jacobsen [28]. We implemented our scheme described in this section with the Γ point approximation. However, even if the size of the C region (with the periodic boundary condition) is large enough to apply the KS-DFT calculation with one k-sampling point, the transmission coefficient and density of states sometimes provide a sharp cusp as a function of energy in the Γ point approximation. One k-sampling with the use of a non-Γ point is useful for eliminating such a cusp, although the Γ point approximation can remove cusps by increasing the cell size sufficiently. In the present system, the C region is not as small as described in the next section, and there is no unphysical behavior caused by the van Hove singularity in the focused energy region. Therefore we adopt the Γ point approximation for the following test calculations. If one needs non-Γ point sampling, our efficient MO approach described in section 2.2 can be extended straightforwardly. Also if one carries out the same procedure with the above $O(N)$ method, but makes supercells which contains more than $N_{\mathrm{cell}} \times N_{\mathrm{cell}}$ cells, one can take the non-Γ sampling point for the self-energy matrix of a $N_{\mathrm{cell}} \times N_{\mathrm{cell}}$ structure system using the constructed supercell as an extended scheme.

3. Application and results

3.1. Computational model

In the present study, we apply our method to a system of atomic gold wires [32–35]. The C region consists of a chain part of six Au atoms, a 2×2 top layer and three additional 3×3 layers of (100) cross section, which connect to the semi-infinite electrodes (see figure 1(a)). The electrodes are incorporated by the self-energy matrices constructed by the surface Green's functions of the 3×3 (100) structure.

The geometry of the (100) layers is fixed with a lattice constant of 4.08 Å, and the distance between each second layer is kept at 21.90 Å. Only the chain and top layers of each side (a total of 14 atoms) are relaxed, and the vibrational modes are calculated in this vibrational box. Here, we note that we take a much larger region (W) than the C region to determine the first derivatives of the Hamiltonian and overlap matrices and the Hessian, although only the parts relating to the C region are explicitly used by clipping the CC block from the whole matrix spanned in the W region like the construction of embedding potential shown in section 2.3. We took the W region as the C region plus the outer three layers. We focus on only the highest alternating bond length (ABL) mode, which is denoted by α and has the highest frequency Ω_{α}. Although we omitted explicit couplings between different phonon modes, the temperature is fixed with 15.0 K, and broadening parameter for the phonon Green's function is set to 20.0 meV.

Part of the DFT calculation was performed by the SIESTA program package [36]. and PBE functions were adopted as the XC functional [37]. The basis set employed is the AO type of the polarized single zeta (SZP) level. The above XC functional and basis functions were also employed for the NEGF–SCF calculation.

3.2. Model (I)

Model (I) is the whole 2D periodic system and represents the physical situation given in figure 1(b). The atoms in the vibrational box hardly changed position after the geometrical

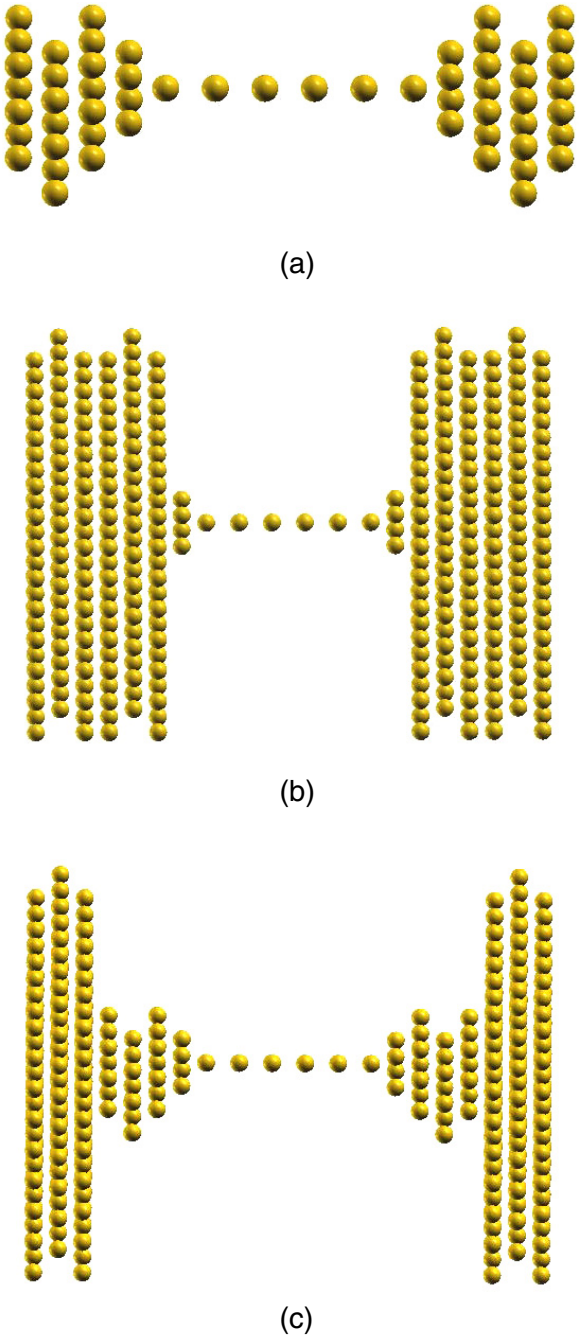

Figure 1. The atomic structure of the gold wire in the Au(100) system. (a) The unit cell of the C region treated with/without the periodic boundary condition in each model, as well as the electrodes. (b), (c) Schematic figures of physical systems corresponding to the adopted periodic (or non-periodic) condition for the C region and the semi-infinite electrodes. Parts (b) and (c) relate to models (I) and (II), respectively, in the text.

(This figure is in colour only in the electronic version)

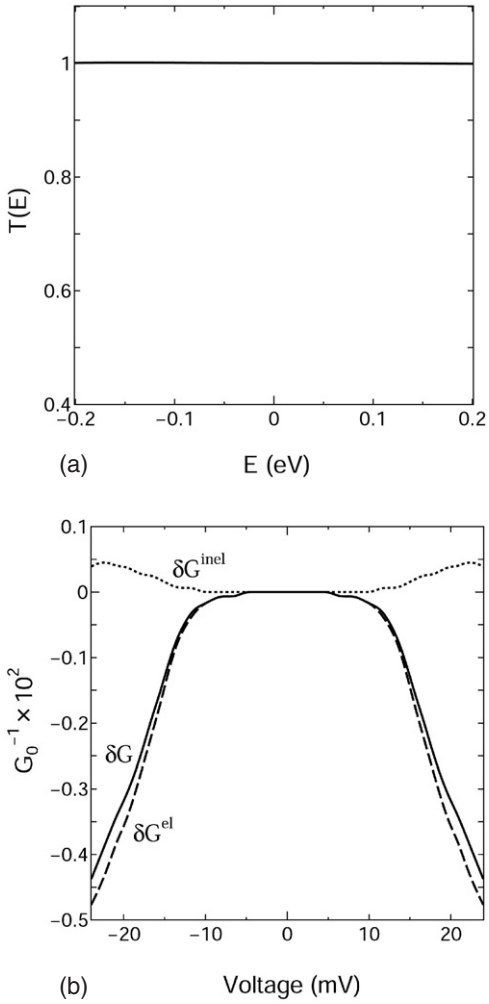

Figure 2. The transmission coefficient $T_0(E)$ and the changes of conductance by electron–phonon scattering in model (I). $T_0(E)$ in the zero-bias limit is plotted as a function of electron energy in (a), where the Fermi level is set to zero. The change of conductance is given as a function of the voltage in (b). The total change δG is shown by the solid line, and elastic ($\delta G^{\rm el}$) and inelastic ($\delta G^{\rm inel}$) terms are given by the dashed and dotted lines, respectively.

optimization, i.e. the chain part is linear, and the structure of the top layers is almost same with a (100) section. Using this optimized geometry, we found that the ABL mode Ω_α is 128.3 cm^{-1}.

The calculated (ballistic) transmission coefficient, $T_0(E)$, was almost constant in the energy range $[-0.2, 0.2$ eV] and has a value of 1.0 due to conduction of the 6s electron of Au at low bias voltage as shown in figure 2(a), where we set the Fermi level to 0. In the present case, we focus on only low applied voltage (typically lower than 25 mV), and the voltage dependence of $T_0(E)$ is quite small. Therefore we only show $T_0(E)$ for the zero-bias case for the all models and illustrate this in the figures.

To get a converged result for the size of the active space, we tried several sets of active MO spaces. We found that the active space, whose MO energies are in $[-0.6, 0.6$ eV] in the zero-bias limit, is sufficient if the applied bias is lower than 0.1 V. The total number of active MOs is only 16 MOs.

The change of conductance caused by electron–phonon scattering, δG, can be defined by the sum of $\delta G^{\rm el}$ and $\delta G^{\rm inel}$, where each term is defined by $\frac{{\rm d}(\delta I^{\rm el})}{{\rm d}V}$ and $\frac{{\rm d}I^{\rm inel}}{{\rm d}V}$, respectively. The resulting terms, δG etc, are illustrated as a function of V in figure 2(b). The elastic term dominates conductance drop, and the decrease is close to linear when the applied bias

is larger than Ω_α. The magnitude of δG is about 0.15% of G_0 at $eV \approx \hbar\Omega_\alpha$, where G_0 is the conductance unit $e^2/\pi\hbar$. The experimental results are within the order of a 0.5–1.5% drop of the conductance [32, 33, 37]: thus our result is a little smaller than the experimental one. However, the shape of δG agrees well with experimental results as a function of the bias voltage. Since the magnitude of the change of conductance is very sensitive to the length of the wire, the distance between the electrodes, and couplings with thermal bath phonons [38], the above agreement will be sufficient to prove the validity of our model. Furthermore, previous theoretical calculations using similar parameters show the same order of magnitude as our result [21, 35]. Comparing with $\delta G^{\rm el}$, the magnitude of $\delta G^{\rm inel}$, which is always a positive value, is close to only 10% of $\delta G^{\rm el}$, and this detailed structure of δG is the same as in theoretical studies [20, 21, 23, 34]. Therefore we conclude that our calculation scheme is also valid.

3.3. Model (II)

In model (II), the lead self-energies are the same as for model (I), but the C region is 1-D non-periodic; thus, the system has a sufficiently long finite cross section on the electrodes. The corresponding physical system is given in figure 1(c). We calculated Ω_α by the same procedure as with model (I). The frequency is very close to that of the 2D contact as well as the eigenmode vector, and the difference in the two frequencies is within only a few $\rm cm^{-1}$. Furthermore, the other eigenmodes in the vibrational box also have similar values to the modes calculated in model (I).

The transmission coefficient $T_0(E)$ for model (II) is presented in figure 3(a). One can find the oscillation structure of $T_0(E)$ in the presented energy window: the minimum value is about 0.7. The position of the Fermi level gives a value close to the bottom of $T_0(E)$. The calculated δG is also plotted as a function of bias voltage in figure 3(b). This is a clear example of waveguide effects due to quantum confinement. In the study by Ke *et al* waveguide effects for tunneling conduction were shown because the bridge part in their study was the benzene–dithiol molecule [22]. The present case shows waveguide effects on open-channel conduction.

The value of δG is about 0.05% of G_0 when the voltage is close to Ω_α; thus, the electron–phonon scatterings affect the conductance drop with a somewhat smaller magnitude for model (II) than for model (I). However, each term resulting from elastic and inelastic scatterings is quite different. Compared with model (I), the magnitude of $\delta G^{\rm el}$ becomes small, and $\delta G^{\rm inel}$ is enhanced. The two values take the same order. Because the inelastic term is directly related to the vibrational heating, the waveguide effects enhance the local heating [35].

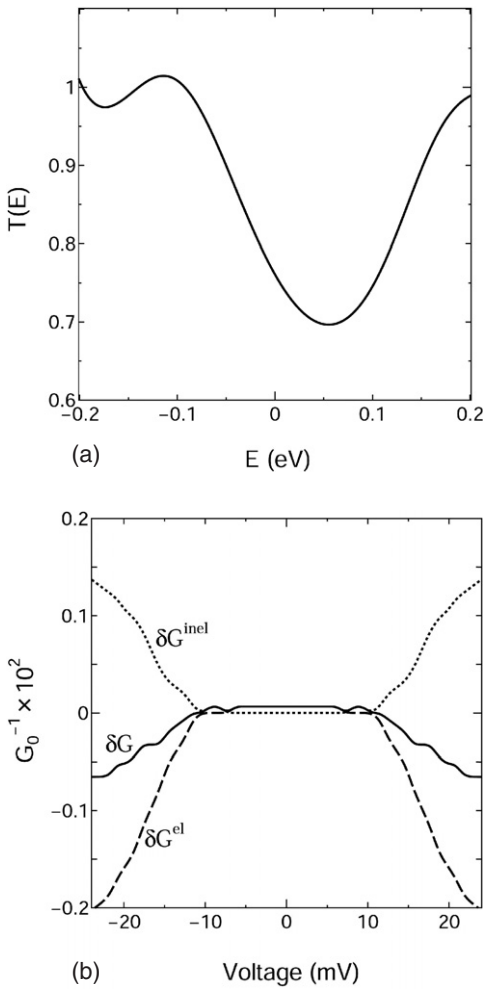

Figure 3. The transmission coefficient $T_0(E)$ and the changes of conductance by electron–phonon scattering in model (II). $T_0(E)$ in the zero-bias limit is plotted as a function of electron energy in (a), and the change of conductance is give as a function of the voltage in (b). The notation is the same as in figure 2.

4. Conclusions

We have proposed a new efficient algorithm to perform the NEGF-DFT procedure and applied it to a gold atomic wire. The improvement of our previous algorithm provides an acceleration of convergence of NEGF-SCF and numerical stability. The scheme has been implemented with inelastic transport processes within the lowest-order perturbation expansion for electron–phonon couplings. The $O(N)$ method to calculate self-energy matrices in the tight-binding-layer scheme is also modified to eliminate unphysical waveguide effects, and satisfactory results were obtained.

Our focus of the application to the case of a gold atomic wire is quantum confinement by finite cross section, and employs two model systems, (I) and (II). The waveguide effects for a small cross section lead to fluctuation in $T_0(E)$ and a large change of the role of conductance by electron–phonon scattering, although the differences in coupling coefficients are relatively small between these models. One of the interesting results in the present study is that the waveguide effects resulting from quantum confinement in physically reasonable situations contribute to $\delta G^{\rm inel}$ more strongly than to $\delta G^{\rm el}$. Because the term $\delta G^{\rm el}$ corresponds to inelastic electron–phonon scattering, which directly relates to vibrational heating, careful theoretical consideration will be required for both structures of the tip/contact and lead parts to analyze vibrational excitations by IETS techniques.

Acknowledgments

This research was supported by a Grant-in-Aid for Scientific Research on Priority Area no. 18041004 from the Ministry of Education, Culture, Sports, Science, and Technology of Japan.

References

[1] Aviran A and Ratner M A 1998 *Molecular Electronics: Science and Technology* (New York: New York Academy of Sciences)
[2] Reed M A, Zhou C, Deshpande M R, Muller C J, Burgin T P, Jones L and Tour J M 1998 *Mol. Electron. Sci. Technol.* **852** 133
[3] Reed M A, Zhou C, Muller C J, Burgin T P and Tour J M 1997 *Science* **278** 252
[4] Rocha A R, Garcia-Suarez V M, Bailey S W, Lambert C J, Ferrer J and Sanvito S 2005 *Nat. Mater.* **4** 335
[5] Kawai M, Komeda T, Kim Y, Sainoo Y and Katano S 2004 *Phil. Trans. R. Soc.* A **362** 1163
[6] Kim Y, Komeda T and Kawai M 2002 *Phys. Rev. Lett.* **89** 126104
[7] Komeda T, Kim Y, Fujita Y, Sainoo Y and Kawai M 2004 *J. Chem. Phys.* **120** 5347
[8] Lorente N, Persson M, Lauhon L J and Ho W 2001 *Phys. Rev. Lett.* **86** 2593
[9] Lorente N, Rurali R and Tang H 2005 *J. Phys.: Condens. Matter* **17** S1049
[10] Ness H and Fisher A J 2005 *Proc. Natl Acad. Sci. USA* **102** 8826
[11] Sainoo Y, Kim Y, Okawa T, Komeda T, Shigekawa H and Kawai M 2005 *Phys. Rev. Lett.* **95** 246102
[12] Stipe B C, Rezaei M A and Ho W 1999 *Rev. Sci. Instrum.* **70** 137
[13] Troisi A and Ratner M A 2006 *J. Chem. Phys.* 125
[14] Brandbyge M, Mozos J L, Ordejon P, Taylor J and Stokbro K 2002 *Phys. Rev.* B **65** 165401
[15] Damle P, Ghosh A W and Datta S 2002 *Chem. Phys.* **281** 171
[16] Nakamura H and Yamashita K 2006 *J. Chem. Phys.* **125** 194106
[17] Rocha A R, Garcia-Suarez V M, Bailey S, Lambert C, Ferrer J and Sanvito S 2006 *Phys. Rev.* B **73** 085414
[18] Taylor J, Guo H and Wang J 2001 *Phys. Rev.* B **63** 245407
[19] Frederiksen T, Brandbyge M, Lorente N and Jauho A P 2004 *Phys. Rev. Lett.* **93** 256601
[20] Paulsson M, Frederiksen T and Brandbyge M 2005 *Phys. Rev.* B **72** 201101
[21] Viljas J K, Cuevas J C, Pauly F and Hafner M 2005 *Phys. Rev.* B **72** 245415
[22] Ke S H, Baranger H U and Yang W T 2005 *J. Chem. Phys.* **123** 114701
[23] Frederiksen T, Paulsson M, Brandbyge M and Jauho A P 2007 *Phys. Rev.* B **75** 129901
[24] Ho K M, Fu C L and Harmon B N 1984 *Phys. Rev.* B **29** 1575
[25] Sergueev N, Roubtsov D and Guo H 2005 *Phys. Rev. Lett.* **95** 146803
[26] Galperin M, Ratner M A and Nitzan A 2007 *J. Phys.: Condens. Matter* **19** 10321
[27] Ness H 2006 *J. Phys.: Condens. Matter* **18** 6307
[28] Thygesen K S and Jacobsen K W 2005 *Phys. Rev.* B **72** 033401
[29] Nakamura H and Yamashita K 2008 to be submitted
[30] Sanvito S, Lambert C J, Jefferson J H and Bratkovsky A M 1999 *Phys. Rev.* B **59** 11936
[31] Damle P S, Ghosh A W and Datta S 2001 *Phys. Rev.* B **64** 6420
[32] Agrait N, Untiedt C, Rubio-Bollinger G and Vieira S 2002 *Phys. Rev. Lett.* **88** 216803
[33] Agrait N, Untiedt C, Rubio-Bollinger G and Vieira S 2002 *Chem. Phys.* **281** 231
[34] Anglada E, Torres J A, Yndurain F and Soler J M 2007 *Phys. Rev. Lett.* **98** 096102
[35] Nakamura H and Yamashita K 2008 *Nano Lett.* **8** 6
[36] Soler J M, Artacho E, Gale J D, Garcia A, Junquera J, Ordejon P and Sanchez-Portal D 2002 *J. Phys.: Condens. Matter* **14** 2745
[37] Perdew J P, Burke K and Ernzerhof M 1996 *Phys. Rev. Lett.* **77** 3865
[38] Frederiksen T, Lorente N, Paulsson M and Brandbyge M 2007 *Phys. Rev.* B **75** 235441